12^{th} International Conference on Fracture Mechanics of Concrete and Concrete Structures
FraMCoS-12
B.L.A. Pichler, Ch. Hellmich, P. Preinstorfer (Eds)

https://doi.org/10.21012/FC12.1223
MS03-2:5

PRECURSORS FOR DETECTING IMPENDING FRACTURE IN CEMENTITIOUS COMPOSITES USING NATURAL TIME ANALYSIS OF ACOUSTIC EMISSION

KASHIF NAUKHEZ[1*], R. VIDYA SAGAR[1†] AND J. M. CHANDRA KISHEN[1††]

[1]Indian Institute of Science, Bangalore 560012, India
e-mail: [1*]kashifn@iisc.ac.in
e-mail: [1†]rvsagar@iisc.ac.in
e-mail: [1††]chandrak@iisc.ac.in

Key words: Natural time analysis, Acoustic emission, Ultra high performance concrete, Impending fracture.

Abstract. This article presents the application of natural time analysis of acoustic emission (AE) to detect impending fracture in ultra high performance concrete (UHPC). The UHPC beams with and without coarse aggregate were made and subjected to a three-point bending test. Simultaneously, the generated AE were recorded using an eight channel AE monitoring system. The parameters, namely, variance (κ_1), entropy (S), and entropy under time reversal (S_-), were studied in natural time domain. All these parameters simultaneously reached their critical values and fluctuated within the time window corresponding to the region of criticality. The critical conditions of the parameters were accompanied by a significant increase in cumulative AE energy, which resembled the Olami-Feder-Christensen earthquake model. Furthermore, change in entropy (ΔS) was minimized before the mainshock event, thus indicating the imminent major event. Therefore, κ_1, S, S_-, and ΔS could be utilized as precursors for detecting impending macroscopic fracture in cementitious composites.

1 INTRODUCTION

It is known that the fracture process in cementitious materials is a complex phenomenon that spans a wide range of spatial and temporal scales [1]. Several experimental studies have shown that the fracture process is governed by scale-invariant laws, namely, Omori's law, productivity law, unified waiting-time scaling law, and the Gutenberg-Richter (G-R) empirical relationship [2, 3]. These laws highlight phenomena that are closely linked to the material's approach to a critical point, reflecting the progressive evolution of damage and the transition from microcracking to its macroscopic failure [4]. A notable example is the acoustic emission (AE) observed before fracture, characterized by the generation of transient elastic stress waves within a solid due to the rapid release of localized strain energy. This phenomenon can be interpreted within the framework of fracture mechanics [5–7]. Analyzing the sources of AE provides insights into the microscopic processes underlying the initiation and progression of damage in cementitious materials [8].

Previous studies have explored the approach of analyzing time series data from AE laboratory tests using the same or modified methods in seismology [9–11]. The aim was to develop precursor parameters to detect impending structural failure [12]. To achieve this, the G-R empirical relation, used in seismology to describe the relationship between the frequency of occurrence and magnitude of seismic events, has been applied to AE signals in materials sci-

ence. In this context, the AE based b-value, which characterizes the distribution of AE peak amplitudes, was introduced under the modified G-R law, providing insights into the underlying mechanisms of damage accumulation and failure in heterogeneous materials [10]. However, b-value analysis faces challenges in fitting the frequency of occurrence-magnitude relationship to the modified G-R law. This is due to the nonlinearity of data, often caused by a lack of high amplitude AE events and incomplete detection of low amplitude events [13]. Few other research studies introduced the Hurst exponent (H) as a precursor failure indicator, which quantifies the long memory characteristics in complex systems. Cisternas et al. [14] and Lee et al. [15] implemented the Hurst exponent to study seismicity trends, focusing on temporal, spatial, or size-related features. Burud et al. [16] investigated long memory characteristics using acoustic emission time series analysis, employing the Hurst exponent to detect damage in concrete under monotonic and fatigue loading. However, H can be influenced by trends or non-stationary data, such as gradual changes in material properties over time, leading to inaccurate estimates in complex systems like concrete.

To address these limitations and extract maximum information from complex time series data, natural time (NT) analysis was introduced by Varotsos et al. [17]. The NT analysis enables the identification of when the complex system enters the critical stage. In this new perspective, novel dynamical features hidden within time series can emerge but cannot be extracted when the analysis is carried out in conventional time [18]. The NT analysis was originally adopted for the analysis of seismic electric signals associated with earthquakes. In the case of seismicity, it has been observed that the mainshock event typically occurs a few days after the parameters associated with the NT analysis fluctuate around a critical value. This, in turn, shortened the time window for the occurrence of a large earthquake [19,20]. Motivated by this, the notion of NT analysis was extended to fracture studies in solids to prevent the catastrophic failure of the specimen. Triantis et al. [18] investigated the existence of critical indices provided by NT analysis in plain and steel fibre reinforced notched TPB specimens. Another study by Friedrich et al. [12, 21] focussed on identifying impending failure in concrete cubes under uniaxial compression by analyzing acoustic emission time series in the NT domain. A comparative assessment was conducted to analyze criticality indices extracted from acoustic and electrical signals in marble specimens, as reported by Kourkoulis et al. [22]. The framework of natural time analysis of AE has also been applied to rocks, cement mortar, and other structural elements [23–25].

Relatively fewer studies focussed on investigating the recorded acoustic emissions before fracture in fibre reinforced cementitious composites subjected to flexural loading under the framework of NT analysis. Therefore, the present study aims to detect the existence of critical indices that can serve as pre-failure indicators, signaling the transition of a mechanically loaded specimen into its critical stage, which signifies the onset of impending fracture. Furthermore, the behavior of the specimen was understood either by the Olami-Feder-Christensen (OFC) model or the Burridge-Knopoff (BK) train model using the obtained NT parameters (κ, S and S_-) [26, 27].

2 METHODOLOGY

2.1 Theoretical background of natural time analysis

For a series of N AE events, natural time (χ_k) for the occurrence of the k^{th} event is $\chi_k = k/N$. This approach ignores the time intervals between consecutive events while retaining their order and the associated energy (E_k). NT analysis is performed by studying the evolution of the pair (χ_k, p_k), where the quantity, p_k, is the normalized energy for the k^{th} event and is [17]:

$$p_k = \frac{E_k}{\sum_{n=1}^{N} E_n} \tag{1}$$

The quantities p_k represent how the ability of a complex system to emit energy changes as k or χ_k increases. It can also be considered as a probability for the occurrence of the k^{th} event at χ_k. In the context of probability theory, information about the distribution of p_k can be derived from the behaviour of the characteristic function, $\Phi(\omega)$

$$\Phi(\omega) = \sum_{k=1}^{N} p_k e^{i\omega\chi_k} \tag{2}$$

where ω is the angular natural frequency.
Using the normalized power spectrum $\Pi(\omega)$, $\Phi(\omega)$ can be expressed as:

$$\Pi(\omega) = |\Phi(\omega)|^2 \tag{3}$$

In NT analysis, the behaviour of $\Phi(\omega)$ is studied at $\omega \to 0$ since all the moments of the distribution of p_k can be obtained from the derivatives $\frac{d^m\Phi(\omega)}{d\omega^m}$ (for m being a positive integer) of the characteristic function $\Phi(\omega)$ at $\omega \to 0$. Accordingly, the variance κ_1 is introduced through the Taylor expansion of $\Pi(\omega) = 1 - \kappa_1\omega^2 + \kappa_2\omega^4 - \cdots$ where,

$$\kappa_1 = \langle\chi^2\rangle - \langle\chi\rangle^2 = \sum_{k=1}^{N} \chi_k^2 p_k - \left(\sum_{k=1}^{N} \chi_k p_k\right)^2 \tag{4}$$

where the term $\sum_{k=1}^{N} \chi_k p_k$ represents the averages calculated with respect to the distribution p_k of the normalized energies.
Another important parameter is the entropy S in natural time, which represents a dynamic entropy, as opposed to the static nature of Shannon entropy [17].

$$S = \langle\chi \ln\chi\rangle - \langle\chi\rangle \ln\langle\chi\rangle \tag{5}$$

where $\langle f(\chi)\rangle = \sum_{k=1}^{N} p_k f(\chi_k)$ is the average value of $f(\chi)$ weighted by p_k, i.e., $\langle\chi\ln\chi\rangle = \sum_{k=1}^{N} p_k(k/N)\ln(k/N)$ and $\langle\chi\rangle = \sum_{k=1}^{N} p_k(k/N)$.

In the stable state of the complex system, E_k behaves as independent and identically distributed random variables, resulting in $p_k \to 1/N$, which is termed as uniform distribution, with S attaining a value of S_u equal to 0.0966. Reversing the time arrow and applying the time reversal operator T to p_k, i.e., $\mathrm{T}p_k = p_{N-k+1}$, results in a change in the value of S, which becomes S_-.

$$\begin{aligned} S_- = &\sum_{k=1}^{N} p_{N-k+1} \frac{k}{N} \ln\left(\frac{k}{N}\right) \\ &- \left(\sum_{k=1}^{N} p_{N-k+1} \frac{k}{N}\right) \ln\left(\sum_{k=1}^{N} p_{N-k+1} \frac{k}{N}\right) \end{aligned} \tag{6}$$

Therefore, S is causal, meaning an operator describing the time evolution of a dynamical system is causal if it depends only on the past values of the time series. In contrast to S, the quantity κ_1 remains unchanged under time reversal, similar to the power spectrum of any time series [17].
Furthermore, a change in entropy, $\Delta S = S - S_-$ in natural time under time reversal can be obtained using equation (5) and equation (6). The quantity ΔS reaches a global minimum before a major event such as an earthquake and, therefore, could also be used as a prefailure indicator [20].

2.2 Estimation of parameters (κ, S, S_- and ΔS)

A time series of AE hits in natural time, with the corresponding AE energy (E_k) for each hit is formed. As a new AE hit occurs, the number of hits in the series increases by one. With each increase in the number of hits, the value of κ_1 is computed for the pairs (χ_k, p_k). In this computation, χ_k is "rescaled" to $\chi_k = k/(N+1)$, and $p_k = E_k / \sum_{n=1}^{N+1} E_n$ is rescaled to account for the energy distribution of the AE hits, where E_k represents the energy of the k^{th} AE hit. This rescaling ensures that the system's evolution is accurately tracked, as each hit contributes to the overall distribution. In other words, the procedure is carried out by incrementally advancing the AE hit by one, updating the corresponding values of χ_k and p_k for each time step. This process is repeated through the entire time series, sliding one AE hit at a time, until the last recorded AE hit is reached. Using this method, the dynamic changes in the energy distribution of AE hits over the time series are captured using the parameters κ, S, S_-, and ΔS.

2.3 Criticality condition of the parameters

It has been experimentally verified that the following three conditions are satisfied before the specimen approaches a critical stage of impending macroscopic fracture [18, 20].

(i) $\kappa_1 = 0.07$

(ii) $S \leq S_u$ and $S_- \leq S_u$

(iii) ΔS reaches a global minimum.

The criticality condition of $\kappa_1 = 0.07$ has been validated for various critical systems, including the Olami–Feder–Christensen (OFC) earthquake model and the Burridge–Knopoff (BK) train model [26, 27]. The behavior of the OFC earthquake model demonstrates that as κ_1 approaches 0.07, the avalanche size grows exponentially with the applied load, as shown in Fig.1a [17]. Furthermore, the analysis of BK train model has revealed that as the system gradually approaches self-organized criticality (SOC), a stage appears where $\kappa_1 = 0.070$ and fluctuates around this value, as shown in Fig.1b [28].

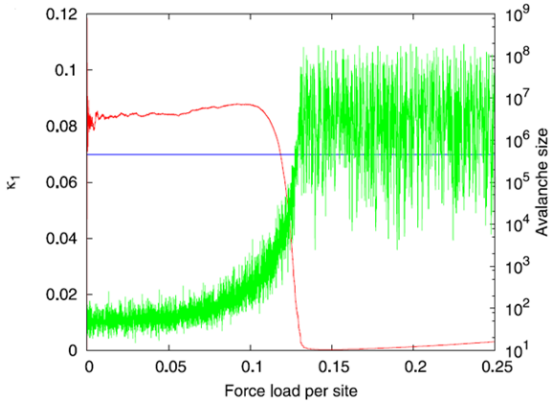

(a)

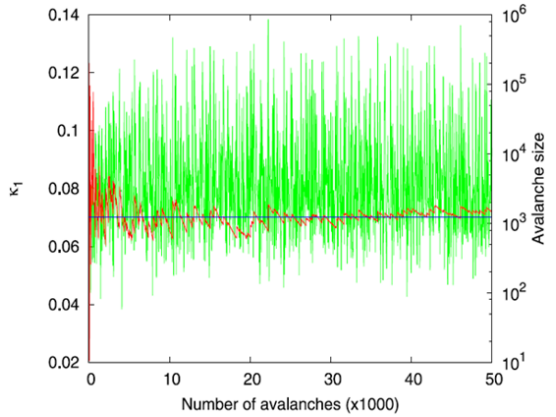

(b)

Figure 1: Results obtained from (a) OFC earthquake model and (b) BK train model for the variance κ_1. [17, 28]

3 EXPERIMENTAL PROGRAM

3.1 Materials and test specimen

Binders (B), namely ordinary Portland cement, blast furnace slag, micro silica, and metakaolin, were used to prepare the UHPC mixture. Basalt stone was used as coarse aggregate (CA) with a nominal maximum size of 12.5 mm, while manufactured sand was used as fine aggregate (FA). The brass coated straight steel fibres with a length of 13 mm, an average diameter of 0.2 mm, and a uniaxial tensile strength of 2950 MPa were used. To improve the workability, a polycarboxylate-ether based superplasticizer (SP) with a specific gravity of 1.122 and a water reduction capacity of 42% was added. A 60 litre capacity pan mixer was used to prepare the UHPC mixture.

Two UHPC mixtures were prepared: UHPC(NCA), without coarse aggregate, and UHPC(CA), with coarse aggregate. A constant water-to-binder (W/B) ratio of 0.18 was maintained for both mixtures. Details of the mixtures are provided in Table 1. For each mixture, three prismatic beams of size 300 mm x 75 mm x 75 mm, conforming to NF P 18-470, were cast. Subsequently, the beams were submerged in a water tank maintained at a temperature of approximately 27°C for 28 days.

Table 1: Mixture details of UHPC mixtures (by weight of binder)

Mixture	B	FA	CA	SF	SP	W/B
UHPC(NCA)	1	1.73	—	0.1	0.015	0.18
UHPC(CA)	1	0.73	0.99	0.1	0.012	0.18

3.2 Test set up

The prismatic beams were subjected to a three-point bending test under displacement control with a loading rate of 0.2 mm/min. The experimental setup consists of a servo-controlled hydraulic loading frame and an eight channel AE monitoring system. Four piezoelectric (PZT) sensors with a resonant frequency of 57 kHz were mounted on the test specimen in a 2D planar layout as depicted in Fig. 2a, while the experimental setup under flexural loading is depicted in Fig. 2b. The preamplifiers were configured with a gain of 40 dB to capture the acoustic emission (AE) activity effectively. To reduce background noise interference, the AE detection threshold was set at 40 dB.

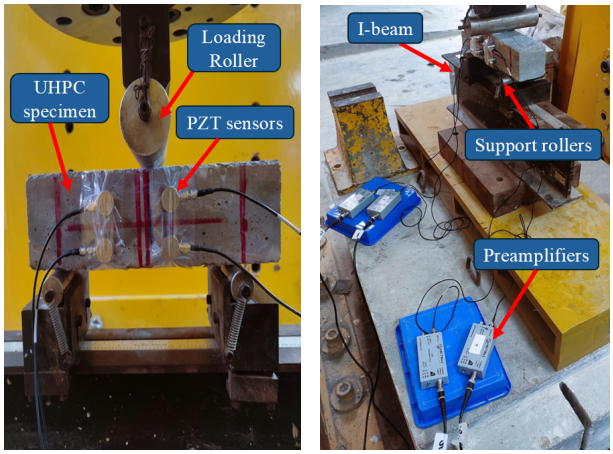

(a) (b)

Figure 2: (a) Planar layout of the PZT sensors (b) Experimental test setup for flexural loading.

4 RESULTS AND DISCUSSION

4.1 Temporal variation of NT parameters, cumulative AE energy and event rate

Fig. 3a shows the variation of parameters (κ, S, S_- and ΔS) in the conventional time for UHPC specimen without coarse aggregate labeled as UHPC(NCA). A region of criticality, which refers to the state of the solid just before it experiences a macroscopic fracture, is marked by a shaded region. This region satisfies the conditions of $\kappa_1 = 0.07$, $S \leq 0.0966$, and $S_- \leq 0.0966$, and is observed between $t \approx 231.8$ s and 259.8 s, corresponding to 84.3% to 93.1% of P_{max}. Here, P_{max} is the peak flexural load of the specimen. Fig. 3b depicts the variation of parameters in the natural time domain for a similar TPB specimen, effectively identifying the region of criticality with χ varying between 0.05 to 0.1. However, the region is less distinguishable in conventional time. The fulfillment of the criticality condition for the parameters indicates that the specimen is approaching a stage of impending macroscopic fracture. To validate this point, the temporal evolution of cumulative AE energy and AE event rate is plotted, as shown in Fig. 3c. The plot is marked with a mainshock event, shown by a vertical dashed line which is distinguished by a peak in the AE event rate and a notable rise in cumulative AE energy. It can be observed that the mainshock event is recorded at 350 s with a corresponding load of 98.8% of P_{max} in the post-peak region. The mainshock event is observed approximately 90 s after the critical conditions of the parameters are satisfied. Furthermore, just after the critical region, an exponential increase in cumulative AE energy is observed. This behavior is similar to the OFC earthquake model, where κ_1 approaches 0.07, and the avalanche size increases exponentially with the applied load, as shown in Fig. 2a. This increase indicates the onset of self-organizing behaviour, which acts as a necessary precursor to failure [25].

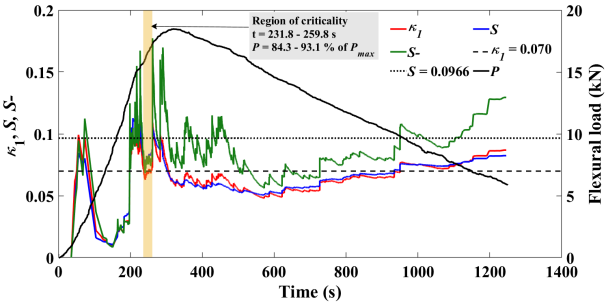

(a)

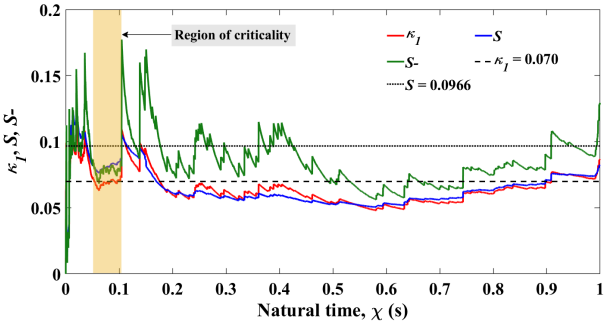

(b)

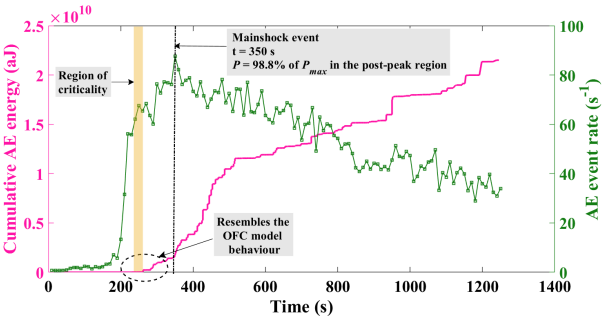

(c)

Figure 3: Results for UHPC(NCA) specimen depicting the variation of parameters, κ_1, S, and S_- in (a) conventional time, (b) natural time domain, along with (c) the temporal evolution of cumulative AE energy and AE event rate.

Fig. 4a shows the variation of parameters in the conventional time for UHPC specimen with coarse aggregate, referred to as UHPC(CA). A region of criticality is observed between $t \approx 289.5$ s and 332.9 s

where the parameters $\kappa_1 = 0.07$, $S \leq 0.0966$, and $S_- \leq 0.0966$ attains its critical value, is indicated by a shaded region. This region corresponds to 99.7% to 97.6*% of P_{max}, where * represents the percentage of load in the post-peak region. Fig. 4b shows the variation of parameters in the natural time, χ ranging between 0.38 to 0.44, where a well-defined region of criticality can be observed. The temporal evolution of cumulative AE energy and AE event rate is shown in Fig. 4c, where the mainshock event occurs at 500 s with a corresponding load of 85.9% of P_{max} in the post-peak region. The mainshock event is observed approximately 167 s after the parameters reach their critical values, which is higher as compared to UHPC(NCA) specimen. This increased time window could be attributed to the enhanced energy dissipation and crack resistance provided by CA. Furthermore, the inclusion of CA increases the heterogeneity of the material by forcing cracks to deviate from their path, consume additional energy, and delay the onset of critical fracture. In addition, it contributes to stress redistribution, resisting crack growth and delaying the coalescence of microcracks. Consequently, the progression towards macroscopic fracture is slower and more controlled in UHPC(CA) as compared to UHPC(NCA). Thus, it can be interpreted that the presence of CA provides an early warning indication of impending macroscopic fracture of the specimen and prevents its catastrophic failure. Fig. 4c depicts a sudden increase in cumulative AE energy, just after the critical region. This behavior resembles the OFC earthquake model, as observed in UHPC(NCA) specimen, where κ_1 approaches 0.07, as shown in Fig. 2a, reflecting the onset of self-organizing behaviour of the material. Moreover, a significant difference between the entropy (S) and the entropy under time reversal (S_-) is observed for both UHPC mixtures. This behavior was theoretically predicted by the OFC earthquake model and has recently been experimentally observed prior to strong earthquakes. However, the characteristics of the BK train model, which exhibit a slight continuous increase in cumulative AE energy, as shown in Fig. 2b, were not observed in any of the UHPC mixtures tested in this study. This suggests a fundamental difference in the fracture behaviour of UHPC compared to the BK train model. Nevertheless, further experimental investigations with a larger number of samples are required to validate this observation.

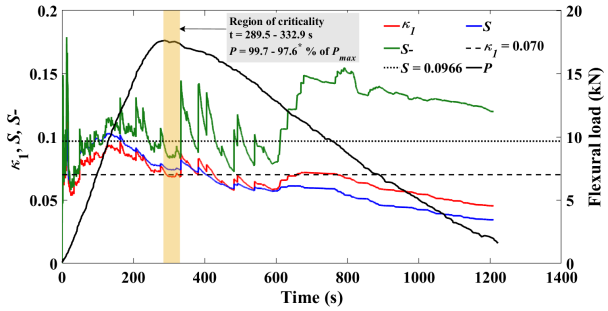

(a)

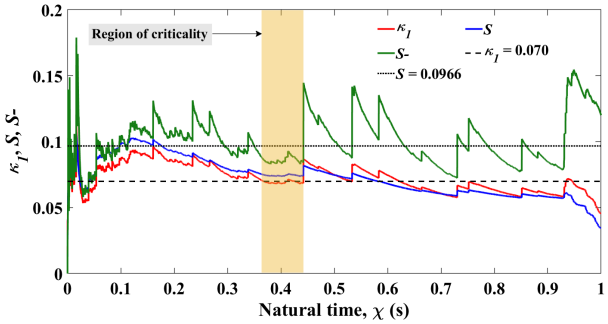

(b)

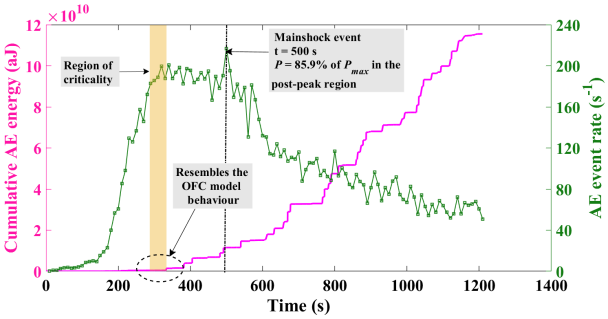

(c)

Figure 4: Results for UHPC(CA) specimen depicting the variation of parameters, κ_1, S, and S_- in (a) conventional time, (b) natural time domain, along with (c) the temporal evolution of cumulative AE energy and AE event rate.

4.2 Temporal variation of change in entropy (ΔS)

Fig. 5a shows the temporal evolution of change in entropy (ΔS) for UHPC(NCA) specimen. It is observed that the ΔS reaches a global minimum, ΔS_{min}, prior to the impending large avalanche, i.e., the mainshock event, thereby indicating the imminent major event. The negative values of ΔS indicate that the avalanche size, or the cumulative AE energy, in this case, tends to increase as the time approaches the mainshock event [17]. A similar observation was noted for UHPC(CA) specimen as shown

in Fig. 5b, where ΔS_{min} is reached prior to the mainshock event. Therefore, it could be stated that the parameters, κ_1, S, and S_-, integrated with ΔS, provide an early warning signal of an impending macroscopic fracture.

NT analysis has been successfully applied in controlled laboratory conditions under monotonic loading, where their ability to detect criticality and impending macroscopic fracture has been demonstrated. However, their applicability under random and occasional loading in practical engineering structures, such as bridges or buildings subjected to variable service loads, requires further investigation. The authors are of the opinion that these parameters can still capture underlying damage evolution trends in non-monotonic loading conditions, provided a sufficient number of AE hits are recorded for accurate estimation. Integrating NT analysis with continuous AE monitoring systems in practical applications could enable real-time damage assessment under fluctuating loads, enhancing structural health monitoring. Additionally, this approach could help in identifying early signs of critical damage, allowing for timely maintenance.

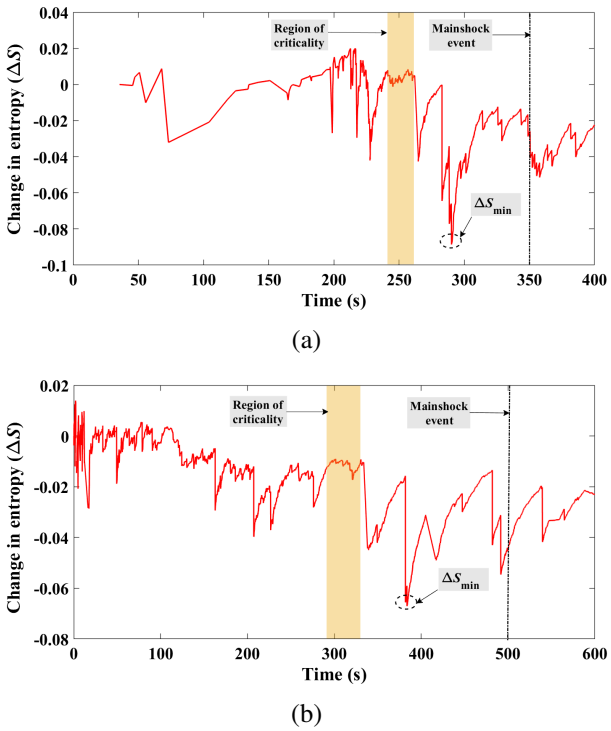

Figure 5: Temporal evolution of change in entropy (ΔS) for (a) UHPC(NCA) and (b) UHPC(CA) specimen.

4.3 Comparison of NT analysis with the AE based b-value

Fig.6a and Fig.6b depicts the variation of AE-based b-value for UHPC(NCA) and UHPC(CA) specimens, respectively. For the UHPC(NCA) specimen, the b-value begins to decrease sharply and reaches its local minimum of 0.79 in the post-peak region, just after the region of criticality identified through NT parameters. This reduction in b-value indicates an increasing dominance of larger AE events, suggesting the transition from microcrack accumulation to macroscopic fracture propagation. The reason for this behavior is attributed to the coalescence of numerous microcracks, leading to the formation of macrocracks, which ultimately govern the failure process. It can be observed that the region of criticality is predicted prior to the time when the b-value attains its lowest value, reinforcing the potential of NT parameters as early warning indicators. In the case of UHPC(CA) specimen, the b-value attains its local minimum of 0.83 in the post-peak region after the mainshock event. This suggests that the presence of coarse aggregate influences crack evolution by altering stress distribution and delaying the complete coalescence of cracks. Furthermore, the criticality region is observed well before the b-value reaches its minimum, emphasizing the robustness of NT parameters in capturing early damage signals across different UHPC mixtures. The distinction in b-value trends between the two specimens highlights the role of coarse aggregate in governing failure mechanisms, suggesting that the interaction between aggregate distribution and fiber reinforcement could significantly influence the fracture behavior of UHPC. Therefore, it is evident that the NT parameters could provide a better estimate of the early warning signs of upcoming macroscopic fracture in cementitious composite materials and prevent its catastrophic failure. Additionally, the AE-based b-value, when used in conjunction with NT analysis, can further enhance the predictive capability by capturing changes in crack evolution and damage progression, offering a more comprehensive approach to structural health monitoring.

Further experimental investigations with a larger number of samples and different loading conditions are required to thoroughly validate the reliability and applicability of NT parameters as precursors to macroscopic fracture, enhancing their predictive capability.

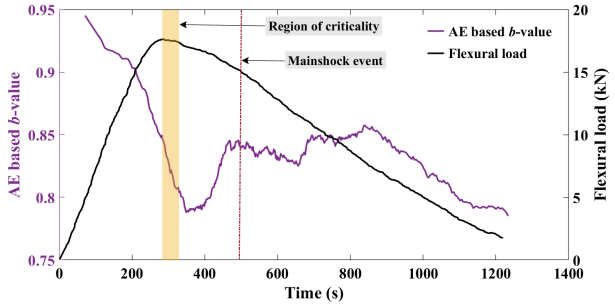

(a)

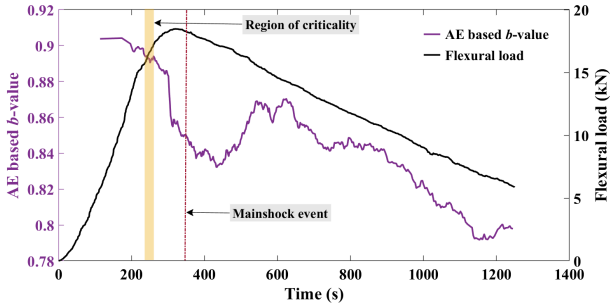

(b)

Figure 6: Comparison of NT parameters with the AE based b-value for (a) UHPC(NCA) and (b) UHPC(CA) specimen.

5 CONCLUSIONS

The natural time analysis of the AE recorded during the three point bending test of UHPC specimens with and without coarse aggregate is presented. The following major conclusions are drawn from the above experimental investigations:

1. The parameters with the critical values of κ_1 = 0.07, $S \leq 0.0966$, and $S_- \leq 0.0966$ effectively identified regions of criticality preceding macroscopic fracture in UHPC specimens.
2. The results align with the Olami-Feder-Christensen (OFC) earthquake model, demonstrating self-organizing behavior in UHPC materials, while the Burridge-Knopoff (BK) train model characteristics were not observed.
3. The temporal evolution of cumulative AE energy and AE event rate provides clear markers for detecting the mainshock event, with a delay observed after the critical conditions are met, particularly in CA specimens.
4. The global minimum of ΔS prior to the mainshock event serves as a reliable indicator of impending macroscopic fracture, consistent across UHPC mixtures.
5. The parameters κ_1, S, and S_-, along with ΔS, serve as early warning indicators of an approaching macroscopic fracture, thereby preventing the catastrophic failure of the specimen.
6. The AE-based b-value could be used in conjunction with NT analysis to enhance the prediction capability by capturing changes in crack evolution and damage progression.

REFERENCES

[1] F. Vallianatos, P. Benson, P. Meredith, and P. Sammonds. Experimental evidence of a non-extensive statistical physics behaviour of fracture in triaxially deformed etna basalt using acoustic emissions. *Europhysics Letters*, 97(5):58002, 2012.

[2] H. J. Herrmann and S. Roux. *Statistical Models for the Fracture of Disordered Media*. Elsevier, Amsterdam, 1990.

[3] Bikas K. Chakrabarti and L. G. Benguigui. *Statistical Physics of Fracture and Breakdown in Disordered Systems*. Oxford University Press, Oxford, 1997.

[4] I. Saha and R. Vidya Sagar. Statistical analysis of acoustic emission avalanches generated during the compressive fracture process and Mode I fracture process in cementitious composites. *International Journal of Fracture*, 234(1–2):273–295, 2022.

[5] D.G. Aggelis, A.C. Mpalaskas, and T.E. Matikas. Investigation of different fracture modes in cement-based materials by acoustic emission. *Cement and Concrete Research*, 48:1–8, 2013.

[6] M. Ohtsu, T. Okamoto, and S. Yuyama. Moment tensor analysis of acoustic emission for cracking mechanisms in concrete. *ACI Structural Journal*, 95(2):87–95, 1998.

[7] M. Ohtsu and K. Ono. Pattern recognition analysis of magneto mechanical acoustic emission signal. *Journal of Acoustic Emissions*, 3:69–80, 1984.

[8] R. Vidya Sagar, B.K. Raghu Prasad, and S. Shantha Kumar. An experimental study on cracking evolution in concrete and cement mortar by the b-value analysis of acoustic emission technique. *Cement and Concrete Research*, 42(8):1094–1104, 2012.

[9] A. Carpinteri, G. Lacidogna, and S. Puzzi. From criticality to final collapse: Evolution of the "b-value" from 1.5 to 1.0. *Chaos, Solitons & Fractals*, 41(2):843–853, 2009.

[10] S. Colombo, I.G. Main, and M.C. Forde. Assessing damage of reinforced concrete beam using "b-value" analysis of acoustic emission signals. *Journal of Materials in Civil Engineering, ASCE*, 15:280–286, 2003.

[11] I Iturrioz, G Lacidogna, and A Carpinteri. Acoustic emission detection in concrete specimens: Experimental analysis and lattice model simulations. *International Journal of Damage Mechanics*, 23(3):327–358, 2013.

[12] L.F. Friedrich, É.S. Cezar, A.B. Colpo, B.N.R. Tanzi, G. Lacidogna, and I. Iturrioz. Identifying impending failure in heterogeneous materials: A study on acoustic emission time series. *Chaos, Solitons & Fractals*, 185:115172, 2024.

[13] Sérgio Luiz E.F. da Silva. k-generalised gutenberg–richter law and the self-similarity of earthquakes. *Chaos, Solitons & Fractals*, 143:110622, 2021.

[14] A. Cisternas, O. Polat, and L. Rivera. The marmara sea region: Seismic behaviour in time and the likelihood of another large earthquake near istanbul (turkey). *Journal of Seismology*, 8(3):427–437, 2004.

[15] Y.-T. Lee, C.-C. Chen, C.-Y. Lin, and S.C. Chi. Negative correlation between power-law scaling and hurst exponents in long-range connective sandpile models and real seismicity. *Chaos, Solitons & Fractals*, 45(2):125–130, 2012.

[16] N.B. Burud and J.M. Chandra Kishen. Investigation of long memory in concrete fracture through acoustic emission time series analysis under monotonic and fatigue loading. *Engineering Fracture Mechanics*, 277:108975, 2023.

[17] Panayiotis A. Varotsos, Nicholas V. Sarlis, and Elias S. Skordas. *Natural Time Analysis: The New View of Time. Precursory Seismic Electric Signals, Earthquakes and Other Complex Time-Series*. Springer, Berlin/Heidelberg, Germany, 2011.

[18] D. Triantis, N.V. Sarlis, A. Loukidis, E.D. Pasiou, I. Stavrakas, and S.K. Kourkoulis. Criticality indices provided by the evolution of pressure stimulated currents and acoustic emissions in the natural time domain. *Theoretical and Applied Fracture Mechanics*, 128:104115, 2023.

[19] P.A. Varotsos, N.V. Sarlis, E.S. Skordas, T. Nagao, and M. Kamogawa. Natural time analysis together with non-extensive statistical mechanics shorten the time window of the impending 2011 tohoku m9 earthquake in japan. *Communications in Nonlinear Science and Numerical Simulation*, 125:107370, 2023.

[20] P.A. Varotsos, N.V. Sarlis, E.S. Skordas, T. Nagao, M. Kamogawa, E.L. Flores-Márquez, A. Ramírez-Rojas, and J. Perez-Oregon. Improving the estimation of the occurrence time of an impending major earthquake using the entropy change of seismicity in natural time analysis. *Geosciences*, 13(8):222, 2023.

[21] L.F. Friedrich, B.N.R. Tanzi, A.B. Colpo, M. Sobczyk, G. Lacidogna, G. Niccolini, and I. Iturrioz. Analysis of acoustic emission activity during progressive failure in heterogeneous materials: Experimental and numerical investigation. *Applied Sciences*, 12(8):3918, 2022.

[22] S.K. Kourkoulis, E.D. Pasiou, A. Loukidis, I. Stavrakas, and D. Triantis. Comparative assessment of criticality indices extracted from acoustic and electrical signals detected in marble specimens. *Infrastructures*, 7(2):15, 2022.

[23] G. Niccolini, G. Lacidogna, and A. Carpinteri. Fracture precursors in a working girder

crane: Ae natural-time and b-value time series analyses. *Engineering Fracture Mechanics*, 210:393–399, 2019.

[24] G. Niccolini, S.M. Potirakis, G. Lacidogna, and O. Borla. Criticality hidden in acoustic emissions and in changing electrical resistance during fracture of rocks and cement-based materials. *Materials*, 13(24):5608, 2020.

[25] A. Loukidis, E.D. Pasiou, N.V. Sarlis, and D. Triantis. Fracture analysis of typical construction materials in natural time. *Physica A: Statistical Mechanics and its Applications*, 547:123831, 2020.

[26] Z. Olami, H.J.S. Feder, and K. Christensen. Self-organized criticality in a continuous, nonconservative cellular automaton modeling earthquakes. *Physical Review Letters*, 68(8):1244–1247, 1992.

[27] R. Burridge and L. Knopoff. Model and theoretical seismicity. *Bulletin of the Seismological Society of America*, 57(3):341–371, 1967.

[28] P.A. Varotsos, N.V. Sarlis, E.S. Skordas, S. Uyeda, and M. Kamogawa. Natural-time analysis of critical phenomena: The case of seismicity. *Europhysics Letters*, 92(2):29002, 2010.